

# Scattering by two degenerate anisotropic modes in square-lattice dielectric photonic crystals

Zhixiang Tang,<sup>1,2</sup> Hao Zhang,<sup>3</sup> Runwu Peng,<sup>1,2</sup> Yunxia Ye,<sup>1</sup> Lei Shen,<sup>1</sup> Shuangchun Wen,<sup>2</sup> and Dianyuan Fan<sup>1</sup>

<sup>1</sup>Shanghai Institute of Optics and Fine Mechanics, The Chinese Academy of Science, Shanghai 201800, People's Republic of China

<sup>2</sup>School of Computer and Communication, Hunan University, Changsha 410082, People's Republic of China

<sup>3</sup>Department of Optical Science and Engineering, Fudan University, Shanghai 200433, People's Republic of China

(Received 15 July 2005; revised manuscript received 29 April 2006; published 7 June 2006)

We systematically investigate the square-lattice dielectric photonic crystals that have been used to demonstrate flat slab imaging experimentally. A right-handed Bloch mode is found in the left-handed frequency region by using the plane wave expansion method to analyze the photonic band structure and equifrequency contours. Using the multiple scattering theory, numerical simulations demonstrate that the left-handed mode and the right-handed mode are excited simultaneously by a point source and result in two kinds of transmitted waves. Impacted by the evanescent waves, superposition of these transmitted waves brings on complicated near field distributions such as the so-called imaging and its disappearance.

DOI: [10.1103/PhysRevB.73.235103](https://doi.org/10.1103/PhysRevB.73.235103)

PACS number(s): 78.20.Ci, 42.30.Wb, 41.20.Jb, 42.70.Qs

## I. INTRODUCTION

Left-handed materials (LHMs), characterized by simultaneous negative permittivity and permeability, were initially proposed and theoretically analyzed by Veselago in the 1960s.<sup>1</sup> Unusual electromagnetic phenomena, such as negative refraction, reversed Doppler shift<sup>2,3</sup> and reversed Cerenkov radiation,<sup>4</sup> could be expected in LHMs. Perhaps the most exciting application of LHMs is the possibility of the superlens.<sup>5</sup>

Due to the absence of nature materials with both negative permittivity and permeability, various approaches have been proposed to fabricate the equivalent metamaterial. Photonic crystal (PhC) is one of these alternatives for its dispersion characteristics. Notomi's theoretical works indicated that left-handed behaviors in PhCs are possible in the regimes of negative group velocity and negative effective index above the first band near the Brillouin-zone (BZ) center.<sup>6</sup> Soon after the experimental observation of negative refraction in PhCs,<sup>7</sup> Parimi *et al.* showed imaging phenomena by flat PhC lenses.<sup>8</sup> They attributed the observed focusing to all-angle negative refraction that could be expected for the LHMs. Using the multiple scattering theory, Ye *et al.* observed the image disappeared when the point source was moved upward by a half lattice constant.<sup>9</sup> Therefore, they did not agree with Parimi but attributed the focusing to the complicated anisotropic scattering. They also analyzed a few other flat slab focusing phenomena in the first partial band gap of the square-lattice PhC, and called them tunneling, self-guiding, or self-collimation effects.<sup>10-13</sup> In this paper we systematically investigate the experimental square-lattice dielectric PhCs.<sup>8,14</sup> A right-handed Bloch mode, which is similar to the self-guiding mode in the first partial band gap, is found in the left-handed frequency region. Using the multiple scattering theory,<sup>12,15</sup> numerical simulations are conducted to demonstrate the left-handed and right-handed modes being excited by quasi-plane waves<sup>15</sup> separately. These two degenerate modes are excited by a point source simultaneously and result in two kinds of transmitted waves. Impacted by the evanescent waves in the near field, superposition of these transmitted waves brings on complicated field distributions near the PhC slabs.

The rest of this paper is organized as follows. In Sec. II, we theoretically analyze the anisotropic characteristics of

these two degenerate modes. Numerical simulations of these two modes being excited by quasi-plane waves separately are demonstrated in Sec. III. The field patterns for the PhC slabs scattered by a point source are given in Sec. IV. Finally, we summarize this paper in Sec. V.

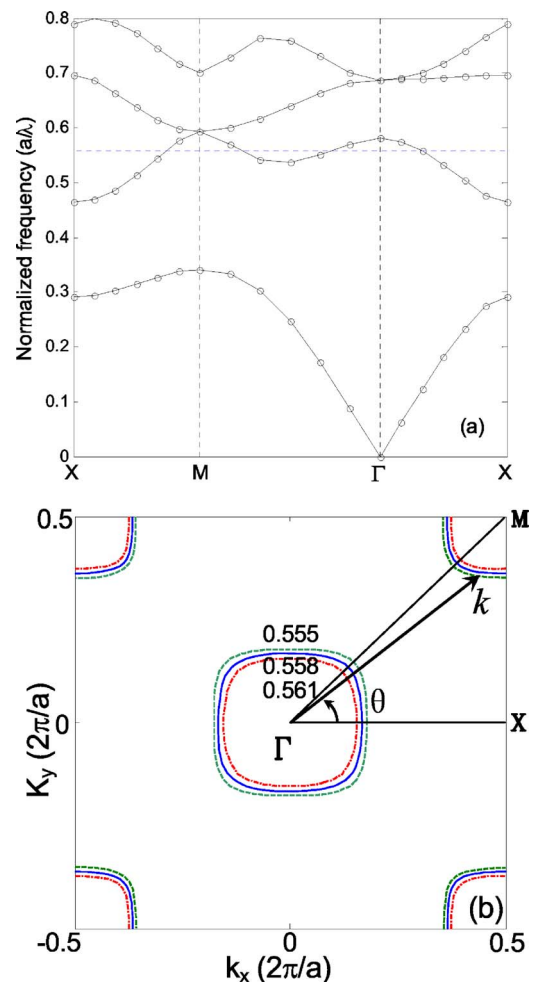


FIG. 1. (Color online) (a) Photonic band structure and (b) EFCs for the 2D PhC studied in this paper.

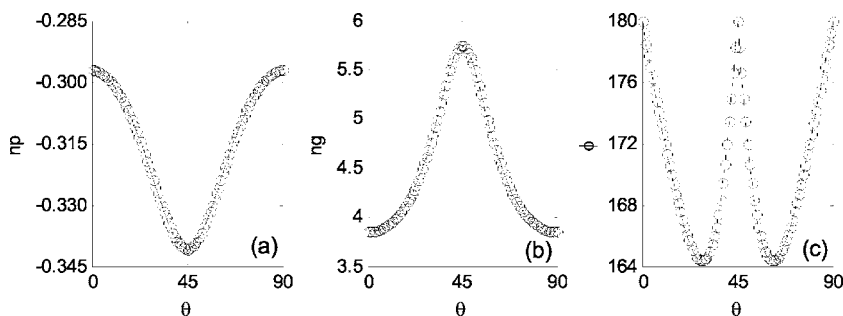


FIG. 2. Schematics for anisotropy analyses of the inner left-handed mode. (a) The phase index  $n_p$ . (b) The group index  $n_g$ . (c) Angles between the Bloch wave vector  $\mathbf{k}$  and its corresponding group velocity  $\mathbf{v}_g$ .

## II. DISPERSION CHARACTERISTICS ANALYSIS

We consider the same system as the experiment:<sup>8</sup> A two-dimension (2D) PhC is formed by a square lattice of dielectric rods with dielectric constant 9.2 (alumina) and excited by the TM mode. The radius of the rods is  $0.175a$ , where  $a$  is the lattice constant. The interface between PhC slab and free space is along  $\Gamma X$ . The photonic band structure as well as equifrequency contours (EFCs) are calculated by the plane wave expansion method and plotted in Fig. 1. All frequencies are normalized as  $a/\lambda$ . In Fig. 1(a) (i.e. the photonic band structure), there are four intersections at the experimental frequency 9.3 G (i.e., normalized frequency 0.558) indicating two degenerate modes. Figure 1(b) shows EFCs of three normalized frequencies 0.555, 0.558, and 0.561. According to Notomi's theories, we can conclude that the inner mode is left-handed and the outer is right-handed.

Considering the symmetry of a square lattice, we calculate the phase and group indices within a quarter of the first BZ to analyze the anisotropic characteristics of these two modes (i.e., the angle  $\theta$  between the wave vector and the interface increases from 0 to  $\pi/2$ ). The phase index<sup>16</sup> can be written as

$$n_p = \mathbf{k}/k_0 = \text{sgn}(\mathbf{k} \cdot \mathbf{v}_g) |\mathbf{k}|/|k_0|, \quad (1)$$

where  $\mathbf{k}$  and  $\mathbf{k}_0$  are the wave vectors of light in PhC and free space, respectively, and sign is the sign function.  $\mathbf{v}_g$  is the group velocity in PhC, which is given by

$$\mathbf{v}_g = \nabla_{\mathbf{k}} \omega(\mathbf{k}). \quad (2)$$

The group index<sup>17</sup> is defined from the group velocity

$$n_g = c/|\mathbf{v}_g| = c/|\nabla_{\mathbf{k}} \omega(\mathbf{k})|, \quad (3)$$

where  $c$  is the velocity of light in free space. Using the plane wave expansion method and Hellman-Feynman theorem,<sup>17</sup> the calculated results of  $n_p$  and  $n_g$  are plotted in Figs. 2 and

3. From these figures, it can be seen that there are superluminal phase velocities ( $n_p < 1$ ) for both modes. But their group velocities are all subluminal ( $n_g > 1$ ) not violating the causality.<sup>18</sup> Because of anisotropy, these indices fluctuate with  $\theta$ .

The angles between the Bloch wave vectors and their corresponding group velocities are calculated and plotted in Figs. 2(c) and 3(c). It is obvious that these two vectors are noncollinear. As shown in Fig. 2(c), for the left-handed mode the phase velocity makes an obtuse angle near  $180^\circ$  with the corresponding group velocity, and these angles fluctuate a little because of almost isotropy. For the right-handed mode in Fig. 3(c), all angles are acute and fluctuate dramatically due to strong anisotropy.

## III. NUMERICAL SIMULATIONS FOR PLANE INCIDENT WAVES

To demonstrate these two degenerate modes being excited by selective plane waves separately,<sup>19</sup> EFC analysis at the experimental frequency  $\omega_0 = 0.558$  is schematically plotted in Fig. 4, where the phase-matching conditions at the incident interface are denoted by dashed lines. Taking the incident beam with an angle  $\alpha$  as an example, the phase-matching conditions indicate two possible refracted Bloch waves that are denoted by  $\Gamma A$  and  $\Gamma A'$ , respectively. Considering the left-handed behavior of the inner mode, only  $\Gamma A$  is chosen for the refracted wave for ensuring energy propagating away from the source. The incident beam with an angle  $\beta$  has been analyzed by the same way and its refracted wave vector is denoted by the real red arrow  $\Gamma B'$ . Their corresponding group velocities are denoted by green vectors  $V_g$  and  $V'_g$  approximately. As shown in Fig. 4, owing to the experimental frequency going beyond the long wave limit, some outer right-handed Bloch waves of the neighboring BZs can be excited also.

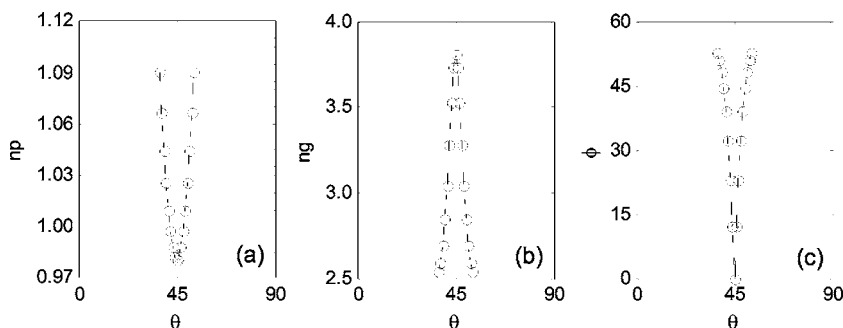


FIG. 3. The same as Fig. 2, but for the outer right-handed mode.

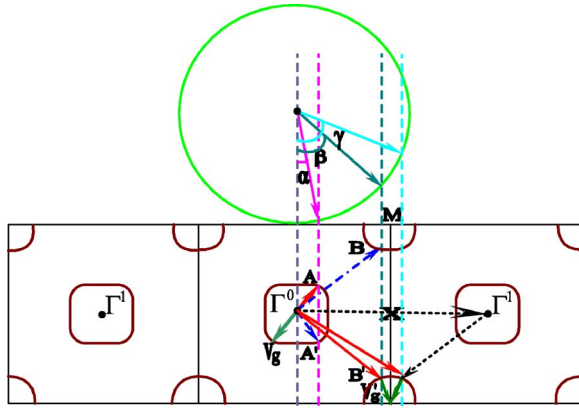


FIG. 4. (Color online) EFCs analyses for plane incident waves. Dashed lines indicate the phase-matching conditions. The excited Bloch wave vector and its corresponding group velocity are denoted by the red and green real arrows, respectively.

In order to test the above analysis, numerical simulations are conducted using the multiple scattering method.<sup>12,15</sup> A slit beam,<sup>15</sup> which is obtained from Kirchhoff integral formula, is taken as the incident quasi-plane wave. As shown in Figs. 5(a) and 5(b), two slit beams with a normalized frequency  $\omega_0=0.558$  are incident to the PhC slab with angles  $\varphi_1=14^\circ$  and  $\varphi_2=50^\circ$  to the normal of the interface, respectively. In Fig. 5(a), the inner left-handed mode is excited and the incident beam refracts negatively with an angle  $\gamma \approx 45^\circ$  to the normal of the interface. As shown in Fig. 5(b), the incident beam refracts positively with an angle  $\gamma \approx 0^\circ$  for the outer right-handed mode being excited. The group velocity makes an angle near  $\phi \approx 50^\circ$  with its phase velocity that is denoted by a red arrow. A Bloch wave of the neighboring BZ excited by an incident beam with an angle  $\varphi_3=70^\circ$  is demonstrated in Fig. 5(c). The incident beam refracts negatively with an angle near  $\gamma \approx 0^\circ$  also. Different from what Ye *et al.* have studied, this kind of self-guiding effect in the PhC slab is along the direction of  $\Gamma X$ . All angles measured in the numerical simulations are close to the theoretical results calculated by the plane wave expansion method in Sec. II. The main discrepancies between the Bloch analysis and numeri-

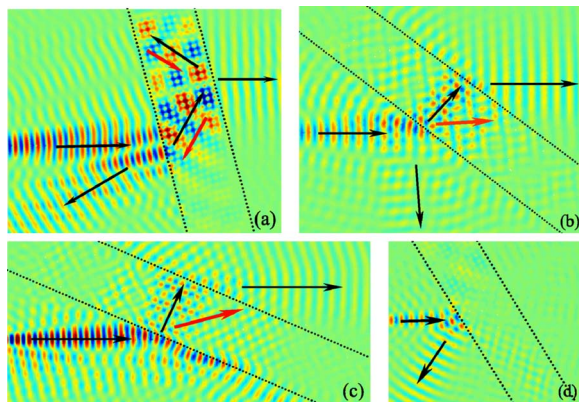


FIG. 5. (Color online) Numerical simulations for slit incident beams with different angles: (a)  $\varphi_1=14^\circ$ ; (b)  $\varphi_2=50^\circ$ ; (c)  $\varphi_3=70^\circ$ ; (d)  $\varphi_4=30^\circ$ . The black and red arrows indicate the group velocities and phase velocities, respectively.

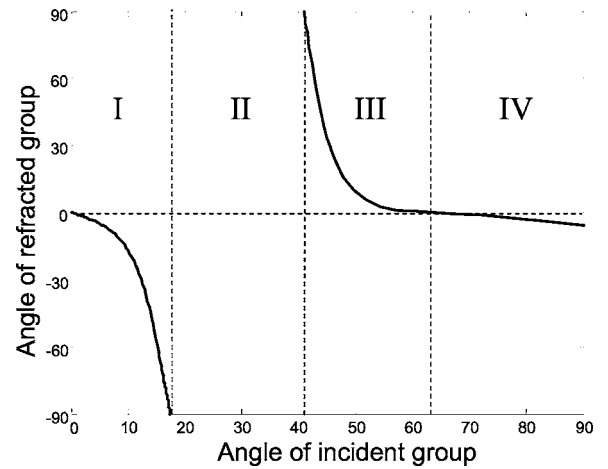


FIG. 6. Schematics for the incident angle in free space and its refracted angle in PhC for the group velocities.

cal simulations can be interpreted with the high spatial frequency components of the incident slit beams.

#### IV. SCATTERING BY A POINT SOURCE

Based on the calculated results in Sec. II, the incident angle in free space and its refracted angle in PhC for the group velocities are plotted in Fig. 6. From this figure, we can see complicated refractions:<sup>19</sup> In part I, i.e., the incident angle  $0^\circ \leq \varphi \leq 17.3^\circ$ , the inner left-handed mode is excited and the incident beam refracts negatively; since no Bloch modes in the PhC are excited in part II ( $17.3^\circ < m < 41^\circ$ ), the incident beam reflects almost totally as shown in Fig. 5(d); in part III ( $41^\circ \leq \varphi \leq 63.6^\circ$ ), the incident beam refracts positively for the outer right-handed mode being excited; the right-handed mode of the neighboring BZ is excited in part IV ( $63.6^\circ < \varphi \leq 90^\circ$ ).

From the above analysis, it is obvious that at the experimental frequency this PhC cannot be treated as an isotropic material by defining an effective index. Actually, when this weakly modulated PhC slab is scattered by a source, the excited evanescent waves are more intricate than that in the long-wavelength limit, and play a very important role in the field distribution such as illustrated in Fig. 5. They are not only responsible for the correct amplitudes of the transmitted and reflected waves in the far field. Having magnitudes comparable to those of the transmitted waves, they also impact the near field distribution directly and dramatically. Although the scattering is very tanglesome, the general regularity can still be concluded on the basis of the Bloch analysis. When this PhC slab is scattered by a point source, these two degenerate modes are excited simultaneously and result in two kinds of transmitted waves. One is the focus formed by the left-handed mode. The other results from the self-guiding effect caused by the right-handed mode. This can be clearly seen from numerical simulations with an elongate PhC slab shown in Figs. 7 and 8. In Fig. 7, all the arrangements are identical to that in the experiment except the PhC slab is elongated to  $10 \times 49$  lattice constant. Similar to Ref. 9, in Fig. 8 the point source is moved upward by a half lattice constant and the PhC slab is added to  $10 \times 50$ . From the field

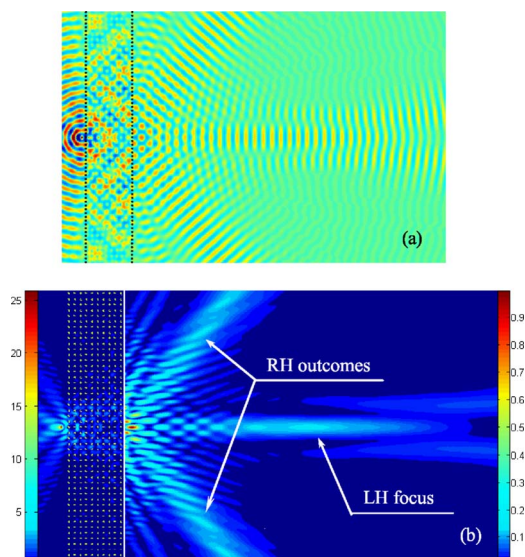


FIG. 7. (Color online) Propagation maps for the PhC slab scattered by a point source: (a) electric field distribution, (b) intensity distribution. All the arrangements are identical to that in the experiment except the PhC slab is elongated to  $10 \times 49$ .

distributions illustrated in these two figures, it is obvious that the images observed in the experiment do not result from the left-handed behavior but the superposition of these transmitted waves near the PhC slabs. The dramatic changes of the near field are basically due to the impact of the evanescent waves, which are sensitive to the source position. In the far field, two kinds of transmitted waves are clearly shown in Figs. 7 and 8.

## V. CONCLUSION

In this paper, we have systematically investigated the experimental square-lattice PhC. A right-handed guiding flow mode, which was omitted before, has been studied. Optical properties of this PhC have been discussed by using the plane wave expansion method to analyze these two degenerate modes. Although the Bloch analyses are obtained for the infinite PhC and the operating frequency goes beyond the long wave limit, these theoretical results are still basically

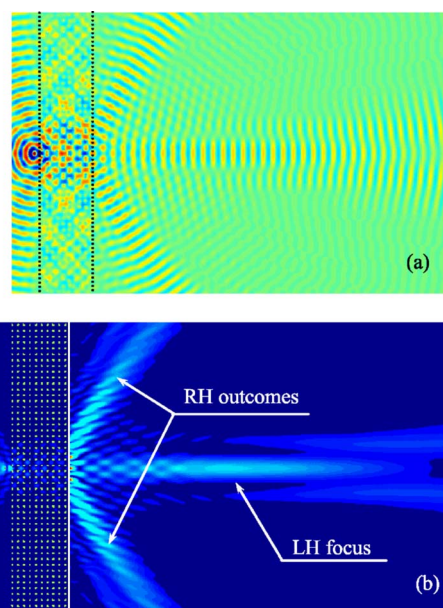


FIG. 8. (Color online) The same as Fig. 7, except the point source is moved upward by a half lattice constant and the PhC slab is added to  $10 \times 50$ .

consistent with the numerical simulations using the multiple scattering method. These so-called images observed in the experiment do not result from the left-handed behavior but the superposition of these two transmitted waves in the near field. These kinds of degenerate modes always coexist in some bands for other PhCs, and our analyses can be extended to them too.

## ACKNOWLEDGMENTS

We thank Xiangdong Zhang for useful suggestion regarding the multiple scattering method. This work is partially supported by the National Natural Science Foundation of China (Grants Nos. 10576012 and 60538010), the National High Technology Research and Development Program of China (Grant No. 2004AA84ts12), and the Specialized Research Fund for the Doctoral Program of Higher Education of China (Grant No. 20040532005).

<sup>1</sup>V. G. Veselago, *Sov. Phys. Usp.* **10**, 509 (1968).

<sup>2</sup>N. Seddon and T. Bearpark, *Science* **302**, 1537 (2003).

<sup>3</sup>E. J. Reed, M. Soljacic, and J. D. Joannopoulos, *Phys. Rev. Lett.* **91**, 133901 (2003).

<sup>4</sup>C. Luo, M. Ibanescu, S. G. Johnson, and J. D. Joannopoulos, *Science* **299**, 368 (2003).

<sup>5</sup>J. B. Pendry, *Phys. Rev. Lett.* **85**, 3966 (2000).

<sup>6</sup>M. Notomi, *Phys. Rev. B* **62**, 10696 (2000).

<sup>7</sup>E. Cubukcu, K. Aydin, E. Ozbay, S. Foteinopoulou, and C. M. Soukoulis, *Nature (London)* **423**, 604 (2003).

<sup>8</sup>P. V. Parimi, W. T. Lu, P. Vodo, and S. Sridhar, *Nature (London)* **426**, 404 (2003).

<sup>9</sup>C.-H. Kuo and Z. Ye, cond-mat/0312288 (unpublished).

<sup>10</sup>C.-H. Kuo and Z. Ye, *Phys. Rev. E* **70**, 056608 (2004).

<sup>11</sup>H.-T. Chien, H.-T. Tang, C.-H. Kuo, C.-C. Chen, and Z. Ye, *Phys.*

*Rev. B* **70**, 113101 (2004).

<sup>12</sup>L.-S. Chen, C.-H. Kuo, and Z. Ye, *Phys. Rev. E* **69**, 066612 (2004).

<sup>13</sup>C.-H. Kuo and Z. Ye, *Phys. Rev. E* **70**, 026608 (2004).

<sup>14</sup>P. Vodo, P. V. Parimi, W. T. Lu, and S. Sridhar, *Appl. Phys. Lett.* **86**, 201108 (2005).

<sup>15</sup>L.-M. Li and Z.-Q. Zhang, *Phys. Rev. B* **58**, 9587 (1998).

<sup>16</sup>H. Kosaka, A. Tomita, T. Kawashima, T. Sato, and S. Kawakami, *Phys. Rev. B* **62**, 1477 (2000).

<sup>17</sup>K. Sakoda, *Optical Properties of Photonic Crystals* (Springer-Verlag, Berlin, 2001).

<sup>18</sup>P. M. Valanju, R. M. Walser, and A. P. Valanju, *Phys. Rev. Lett.* **88**, 187401 (2002).

<sup>19</sup>R. Zengerle, *J. Mod. Opt.* **34**, 1589 (1987).